HHS Public Access

Author manuscript

Neuron. Author manuscript; available in PMC 2018 March 22.

Published in final edited form as:

Neuron. 2017 March 22; 93(6): 1451–1463.e4. doi:10.1016/j.neuron.2017.02.033.

Parvalbumin Interneurons Modulate Striatal Output and Enhance Performance during Associative Learning

Kwang Lee[1,*], **Sandra M. Holley**[2,*], **Justin L. Shobe**[1], **Natalie C. Chong**[3], **Carlos Cepeda**[2], **Michael S. Levine**[2], and **Sotiris C. Masmanidis**[1,4,5]

[1]Department of Neurobiology, University of California, Los Angeles, Los Angeles, California, 90095, USA

[2]Intellectual and Developmental Disabilities Research Center, Brain Research Institute, Semel Institute for Neuroscience & Human Behavior, David Geffen School of Medicine, University of California, Los Angeles, Los Angeles, California, 90095, USA

[3]Neuroscience Interdepartmental Program, University of California, Los Angeles, Los Angeles, California, 90095, USA

[4]California Nanosystems Institute, University of California, Los Angeles, Los Angeles, California, 90095, USA

[5]Integrative Center for Learning and Memory, University of California, Los Angeles, Los Angeles, California, 90095, USA

SUMMARY

The prevailing view is that striatal parvalbumin (PV)-positive interneurons primarily function to downregulate medium spiny projection neuron (MSN) activity via monosynaptic inhibitory signaling. Here, by combining *in vivo* neural recordings and optogenetics, we unexpectedly find that both suppressing and over-activating PV cells attenuates spontaneous MSN activity. To account for this, we find that in addition to monosynaptic coupling, PV-MSN interactions are mediated by a competing disynaptic inhibitory circuit involving a variety of neuropeptide Y-expressing interneurons. Next we use optogenetic and chemogenetic approaches to show that dorsolateral striatal PV interneurons influence the initial expression of reward-conditioned responses, but that their contribution to performance declines with experience. Consistent with this, we observe with large-scale recordings in behaving animals that the relative contribution of PV cells on MSN activity diminishes with training. Together, this work provides a possible mechanism by which PV interneurons modulate striatal output and selectively enhance performance early in learning.

CORRESPONDING AUTHOR AND LEAD CONTACT: Sotiris C. Masmanidis, smasmanidis@ucla.edu.

*Co-first author.

AUTHOR CONTRIBUTIONS: K.L., S.M.H., C.C., M.S.L. and S.C.M. conceived the experiments and wrote the manuscript. K.L., S.M.H., J.L.S., and N.C.C. carried out experiments. All authors analyzed data.

eTOC BLURB

Lee et al. show that striatal PV cells normally enhance striatal output, but are capable of suppressing output, via competing inhibitory microcircuits. They show that the relative contribution of PV cells on striatal activity and behavioral performance diminishes with experience.

INTRODUCTION

The ability to anticipate rewarding events with appropriately timed actions requires neural systems for learning and expressing associations between stimuli and rewards (Day and Carelli, 2007; Fanselow and Wassum, 2015; Graybiel, 2008; Schultz, 2000). The striatum is a major information processing hub and site of plasticity for a variety of reward-conditioned behaviors (Balleine et al., 2007; Gerfen and Surmeier, 2011; Kreitzer and Malenka, 2008; Liljeholm and O'Doherty, 2012; Silberberg and Bolam, 2015; Yin and Knowlton, 2006). In recent years much attention has been drawn toward unveiling the function of direct and indirect pathway projection neurons in movement (Barbera et al., 2016; Cui et al., 2013; Kravitz et al., 2010; Oldenburg and Sabatini, 2015; Rothwell et al., 2015; Tecuapetla et al., 2016; Yttri and Dudman, 2016), reinforcement (Kravitz et al., 2012; Vicente et al., 2016), and sensory processing (Reig and Silberberg, 2014; Sippy et al., 2015). In comparison, the role of inhibitory striatal interneurons in these behavioral functions is less well understood (Fino and Venance, 2011; Kreitzer and Malenka, 2008; Tepper et al., 2010).

A population of GABAergic fast spiking, parvalbumin (PV)-positive interneurons (FSIs) is believed to have an important regulatory role in striatal microcircuits (Berke, 2011; Gittis et al., 2011b; Xu et al., 2016). PV-positive interneurons are concentrated in the dorsolateral striatum (DLS) (Luk and Sadikot, 2001), a subregion that mediates motor skill learning (Graybiel and Grafton, 2015; Yin and Knowlton, 2006) and conditioned responding to reward-associated stimuli (Corbit and Janak, 2007, 2010; Han et al., 1997). Despite a considerable literature on the properties of striatal FSIs based on anatomical studies (Kita et al., 1990), *in vitro* physiology (Tepper et al., 2010), computational models (Damodaran et al., 2014; Gittis et al., 2011a; Hjorth et al., 2009; Humphries et al., 2009; Lau et al., 2010; Moyer et al., 2014), and recordings in behaving animals (Bakhurin et al., 2016; Gage et al., 2010; Schmitzer-Torbert and Redish, 2008; Thorn and Graybiel, 2014; Yamada et al., 2016), their involvement in reward-guided behavior has not been extensively studied with cell type-specific manipulations. Since this type of interneuron is monosynaptically coupled to MSNs (Koos and Tepper, 1999), the normal function of PV cells is thought to strongly involve feedforward inhibition of projection neuron activity (Burguiere et al., 2013; Mallet et al., 2005; Qi et al., 2016). However, because of potential interactions with other types of striatal interneurons (Gittis et al., 2010; Planert et al., 2010; Straub et al., 2016; Szydlowski et al., 2013), an open question is whether the net effect of striatal PV cells is to inhibit or amplify MSN activity.

To understand how PV interneurons influence MSN activity, we performed *in vivo* recordings to examine striatal microcircuit responses to optogenetic PV cell suppression or over-activation. Unexpectedly, both types of manipulations reduced spontaneous MSN

firing. Using *in vitro* measurements we identified a novel disynaptic circuit involving neuropeptide Y (NPY)-containing interneurons, primarily the variety known as neurogliaform (NGF) cells (Ibanez-Sandoval et al., 2011). This disynaptic microcircuit may be a possible, though not exclusive, mechanism by which suppressing PV interneurons reduces MSN firing. Next, to examine the effect of DLS PV interneurons on reward-conditioned behavior, we manipulated these cells in mice learning a Pavlovian stimulus-reward association task. We found that suppressing PV cell activity disrupted conditioned responses, with a selective deficit in the early stage of learning. Finally, to gain insight into why PV interneurons influence behavior in an experience-dependent manner, we combined large-scale neural recordings and optogenetics in animals undergoing reward conditioning. We found that PV interneurons have the greatest impact on neural coding during the initial stage of training. Together, this work reveals two novel and related functions of PV interneurons: to amplify striatal output, and enhance performance early in learning.

RESULTS

PV Interneurons Regulate Spontaneous Striatal Activity

We first examined the effect of suppressing PV neurons on spontaneous firing activity by expressing the hyperpolarizing light-gated proton pump Archaerhodopsin (Arch) (Chow et al., 2010) in the dorsolateral striatum of PV-Cre knockin mice (Figures 1A, S1A, S1B) (Hippenmeyer et al., 2005). We constructed an opto-microprobe device to record from large populations of neurons during optogenetic perturbations (see Experimental Procedures and Figure 1B). The opto-microprobe contained a 256 electrode array enabling recordings from dozens of striatal neurons (Bakhurin et al., 2016), concurrently with local optogenetic manipulations in awake head-fixed mice. Neuronal units were classified as putative MSNs, FSIs, or tonically active neurons (TANs) based on electrophysiological properties (see Experimental Procedures and Figures 1C, 1D).

The average firing rate of putative FSIs decreased during optical stimulation in a laser power-dependent manner (Figure 1E, left and middle; n = 31 FSIs, one-way ANOVA, $F_{4,120} = 4.3$, $p = 0.003$), with the majority of FSIs being negatively modulated by light (Figure 1E, right, signed-rank test, $p < 0.0001$). Since PV cells are known to provide feedforward inhibition onto striatal projection neurons (Koos and Tepper, 1999), we initially expected that this suppression would disinhibit MSNs and increase their firing rate. But surprisingly, the majority of recorded MSNs responded to optical stimulation with a reduction in firing rate (Figure 1F; n = 176 MSNs). The magnitude of this response scaled with the intensity of light. We found that the amount of MSN firing rate modulation was not significantly correlated with their recorded position along the dorsal-ventral axis (Figure S1C, $r = 0.14$, $p = 0.07$), suggesting that MSN suppression occurred approximately uniformly across the opto-microprobe electrode array. We also observed a brief increase in activity of some MSNs at the onset of the optical stimulus. However, we found the same type of transient activity increase in GFP-expressing control mice (Figure 1G; n = 57 MSNs), suggesting that this is an optical stimulus artifact independent of the optogenetic manipulation.

To examine what effect PV interneurons have on principal neuron activity in cortical microcircuits, we carried out Arch stimulation experiments in the prefrontal cortex (see

Experimental Procedures). In contrast to the effects seen in the striatum, we found that suppressing prefrontal cortical PV interneurons caused an increase in principal neuron activity, in line with the expected disinhibitory effect in the cortex (Figure S2A; n = 80 pyramidal cells). These results indicate that, on average, PV interneurons exert opposite effects on principal neuron activity in striatal versus cortical microcircuits.

The action of Arch on presynaptic terminals has been implicated in neurotransmitter release (Mahn et al., 2016). To rule out any such effects in our study we also carried out experiments using the chloride pump Halorhodopsin (eNpHR3.0) (Gradinaru et al., 2008), and observed qualitatively the same trends as with Arch, whereby optical stimulation reduced the spontaneous firing of most MSNs in a laser power-dependent manner (Figure S2B; n = 93 MSNs).

If there is a significant imbalance in DLS PV cell connectivity with direct and indirect pathway MSNs (Gittis et al., 2010), suppression of PV cells may lead to a net reduction in cortical activity, and subsequently, negative feedback with the DLS. This process may represent a mechanism by which suppressing PV cells reduces MSN firing. To examine this possibility we optogenetically suppressed DLS PV cells while simultaneously recording spontaneous activity in the secondary motor cortex, an area which projects to the DLS (Hintiryan et al., 2016) (Figure S2D). We found that optical stimuli did not significantly alter average pyramidal cell firing (Figure S2E, signed-rank test, $p = 0.18$), suggesting that a negative feedback loop of the DLS with this specific cortical region may not explain our results. Instead, our data suggest that the reduction of MSN activity may be due to local microcircuit mechanisms.

Finally, we examined the effects of optogenetically activating PV cells using the depolarizing ion channel Chrimson (Klapoetke et al., 2014). Here the average firing rate of FSIs increased during optical stimulation in a laser power-dependent manner (Figure 1H, left and middle; n = 34 FSIs, one-way ANOVA, $F_{4,132} = 2.6$, $p = 0.04$), even though FSIs were equally likely to be positively and negatively modulated by light (Figure 1H, right, signed-rank test, $p = 0.77$). This manipulation again led to a potent suppression of spontaneous MSN activity (Figure 1I; n = 277 MSNs). Therefore, both suppressing and over-activating DLS PV-expressing cells reduces MSN activity. Together, these results demonstrate that PV interneurons enhance spontaneous MSN firing under physiological conditions (since suppressing PV cells reduces MSN activity), but are also capable of inhibiting MSN firing if they are over-activated.

A Disynaptic PV-NPY-MSN Inhibitory Microcircuit

These findings suggest that in addition to controlling striatal output via monosynaptic coupling mechanisms (Koos and Tepper, 1999), PV cells indirectly couple to MSNs via another type of GABAergic interneuron. This hypothetical disynaptic inhibitory microcircuit would oppose the effects of feedforward monosynaptic inhibition, and enable reduction of MSN activity via PV cell suppression. We speculated that the source of this disynaptic coupling could be neuropeptide Y-containing inhibitory interneurons, because the NGF variety of NPY cells was shown to strongly inhibit MSNs *in vitro* (English et al., 2012; Ibanez-Sandoval et al., 2011). In order to determine whether PV interneurons couple to NPY

interneurons, we recorded from cells using whole-cell patch clamp electrophysiology in brain slices of PV-Cre mice crossed with NPY-GFP mice, and used viral injections to selectively express channelrhodopsin (ChR2) in PV interneurons. Current-clamp recordings of PV interneurons expressing ChR2 showed that injection of depolarizing current pulses induced high-frequency firing in these cells (Figure 2A). Similarly, optically activating ChR2-expressing cells with blue light (0.5 ms, 470 nm, 3 mW) depolarized PV interneurons thereby producing action potentials that occurred within 0.3 ms of the light pulse (Figure 2A, inset).

After determining the effectiveness of optically activating PV interneurons, we recorded optically evoked inhibitory postsynaptic currents (IPSCs) in voltage-clamp mode from MSNs and fluorescently labeled NPY interneurons (Figure 2B). Recordings were only performed on cells that were located within 150 μm of ChR2-expressing striatal PV interneurons that were identified by visible cell surface expression of EYFP fluorescence. All MSNs recorded (7/7) produced IPSCs upon optical stimulation consistent with the high degree of connectivity between PV interneurons and MSNs (Koos and Tepper, 1999). Furthermore, optically evoked IPSCs in MSNs had the greatest amplitude when compared to responses recorded in NPY cells (Figures 2B, 2C). Importantly, optically evoked IPSCs also were detected in fluorescently labeled NPY interneurons. These neurons were divided into two subpopulations, NGF and persistent low-threshold spiking (PLTS) varieties, that were distinguished by the significantly higher membrane input resistance in NPY-PLTS interneurons compared with that in NPY-NGF interneurons (1517.5 ± 131.8 MΩ in NPY-PLTS cells, n = 8; versus 198.1 ± 24.9 MΩ for NPY-NGF cells, n = 9; unpaired t-test, $p < 0.001$). Optical activation of PV interneurons produced IPSCs in all recorded NGF cells (9/9) but only in 62.5% (5/8) of NPY-PLTS cells, suggesting PV cells preferentially connect to NGF over PLTS cells. In addition, optically evoked IPSCs in NPY-NGF cells had significantly higher amplitudes, larger areas and longer decay times compared to responses in NPY-PLTS cells (Figure 2C). All optically evoked IPSC responses in recorded cells had similarly short latencies (2.8 ± 0.1 ms for MSNs, 3.3 ± 0.3 ms for NPY-NGF cells, 3.5 ± 0.4 ms for NPY-PLTS cells) suggestive of direct, monosynaptic connections to PV interneurons. Together, these findings reveal that striatal PV interneurons can directly influence the output of NPY-NGF interneurons, confirming the existence of a disynaptic inhibitory microcircuit that is likely to oppose the effects of monosynaptic (PV to MSN) interactions (Figure 2D). Finally, to show that NPY interneurons are also capable of suppressing MSNs *in vivo*, we performed opto-microprobe recordings in NPY-Cre mice. We found that optogenetically activating NPY cells robustly lowered spontaneous MSN firing (Figure 2E; n = 49 MSNs).

We also examined whether other types of disynaptic striatal circuits could contribute to our results in Figure 1. It is known that striatal FSIs are coupled to each other (Gittis et al., 2010), raising the possibility that PV-PV interactions invert the sign of inhibition on MSNs. A predicted consequence of such interactions is that during optogenetic suppression of a subpopulation of PV cells, a significant portion of recorded FSIs should be disinhibited. However, our data does not support this prediction, as most FSIs were negatively modulated by light (Figure 1E, right). Thus, it is unlikely that interactions between PV cells can explain why suppressing PV interneurons reduced MSN activity. On the other hand, our data do not rule out the importance of PV-PV interactions under conditions when these cells are

synchronously over-activated (Figure 1H, right). Next we examined TANs, which are thought to correspond to cholinergic interneurons (Bennett and Wilson, 1999). Even though these cells are not themselves GABAergic, they are thought to be capable of reducing MSN firing via at least two distinct inhibitory microcircuits (English et al., 2012; Nelson et al., 2014). However, our data showed that suppressing PV cell activity did not significantly alter TAN firing (Figure S2C; n = 24 TANs), implying that TANs are not widely innervated by PV cells. This is in agreement with previous studies showing little or no connectivity between these cells (Gittis et al., 2010; Silberberg and Bolam, 2015; Szydlowski et al., 2013).

PV Interneurons Influence Performance in the Initial Stage of Reward Conditioning

Since PV interneurons regulate striatal output, we hypothesized that they have a role in shaping behavioral performance in striatal-dependent tasks. To test this hypothesis, we bilaterally expressed Arch or Chrimson in DLS PV cells. We then applied bilateral optical stimulation to suppress or over-activate PV cells, while training food-restricted head-fixed mice on a Pavlovian stimulus-reward association task (see Experimental Procedures and Figures S3A and S3B) (Cohen et al., 2012; Shobe et al., 2015). An olfactory conditioned stimulus (CS+) was paired with the delivery of a reward after a 3 s delay, and a neutral stimulus (CS-) was unrewarded. We monitored behavioral output in the form of cue-evoked licking and rotational motion on a circular treadmill. The optical stimulus had a duration of 5 s starting at the olfactory cue offset time (Figure 3A). Under control conditions (GFP^+ mice receiving identical optical stimuli), animals readily acquired an anticipatory licking response during the delay period between the CS+ and reward. This conditioned behavior was consistent with the expression of a learned stimulus-reward association (Cohen et al., 2012). The emergence of conditioned anticipatory licking was significantly delayed when PV cells were either optogenetically suppressed or over-activated (Figure 3B). This unidirectional form of behavioral control by PV interneurons was qualitatively consistent with our electrophysiological data showing that both types of manipulations attenuated spontaneous MSN activity. But critically, by tracking behavior across 3 days of training we found that the contribution of PV interneurons depended on experience. Specifically, we found that suppressing PV cells with Arch had the most significant impact on hit rate (the fraction of CS+ trials with anticipatory licking) on the first day, and no effect by the third day; in contrast, Chrimson-mediated activation had a persistent effect on hit rate (Figure 3C; n = 8 animals per group; two-way ANOVA, group effect: $F_{2,21} = 15$, $p < 0.0001$; time effect: $F_{2,42} = 43.7$, $p < 0.0001$). These results demonstrate that PV interneurons are sufficient to disrupt conditioned responding at any stage of training, but that they are normally only necessary for this behavior early in learning.

We next showed that optical stimulation did not affect the false alarm rate (the fraction of CS − trials with licking), demonstrating that the reduction in hit rate is not due to mice generalizing between CS+ and CS− cues (Figure 3D; two-way ANOVA, group effect: $F_{2,21} = 1.7$, $p = 0.22$; time effect: $F_{2,42} = 6.6$, $p = 0.003$). Furthermore, the reduction in anticipatory licking was not due to a suppression of animals' ability to lick in general, because mice in all groups consumed rewards at an equal rate (Figure S3C; two-way ANOVA, group effect: $F_{2,21} = 0.3$, $p = 0.73$; time effect: $F_{2,42} = 8.1$, $p = 0.001$).

Additionally, we examined whether altering PV cell activity altered cue-evoked motion as measured by the animal's rotation on the treadmill. Suppressing PV interneurons had no effect on treadmill speed, whereas over-activating these cells had a modest effect on the third day of training (Figure S3D; two-way ANOVA, group effect: $F_{2,21} = 2.9$, $p = 0.08$; time effect: $F_{2,42} = 1.7$, $p = 0.2$). Our results suggest that PV interneurons are sufficient to modestly disrupt cued treadmill motion if they are over-activated, but that they normally do not participate in such movement.

One potential explanation for the lack of a hit rate deficit in the late stage of training is that mice learn to compensate for the suppression of PV interneurons over several days of optogenetic stimulation. To examine this possibility we trained a separate Arch-expressing cohort without applying any laser for the first 3 days of training, and monitored behavior both with and without optical stimulation in the middle of day 4. In these animals, we found that the hit rate was not significantly affected by optical stimulation (Figure 3E; n = 8 $Arch^+$ animals; oneway ANOVA, $F_{2,14} = 2.5$, $p = 0.12$). These results rule out compensatory effects of repeated optogenetic stimulation as the cause of the observed experience-dependent decline in the behavioral contribution of PV interneurons. Moreover, inhibiting DLS output by over-activating PV cells for the first time on day 4 of training, reduced the hit rate (Figure S3E, n = 6 $Chrimson^+$ animals; one-way ANOVA, $F_{2,10} = 10.8$, $p = 0.003$). This demonstrates that the DLS remains necessary for expressing the conditioned licking behavior even after learning has taken place (Sippy et al., 2015).

To examine the robustness of the experience-dependent decline in performance upon optogenetic suppression, in another cohort we expressed the inhibitory designer receptor hM4D (Armbruster et al., 2007) in DLS PV cells, and trained naïve mice for 3 days under clozapine N-oxide (CNO) or saline conditions. In agreement with the optogenetic results we found that CNO-treated mice had significantly lower hit rate than controls in the early, but not late stage of training (Figure 3F; n = 7 animals per group; two-way ANOVA, group effect: $F_{1,12} = 8.2$, $p = 0.014$; time effect: $F_{2,24} = 20.8$, $p < 0.0001$). As with optogenetic inactivation experiments, there was no effect on false alarm rate (Figure 3G; two-way ANOVA, group effect: $F_{1,12} = 1.4$, $p = 0.25$; time effect: $F_{2,24} = 7$, $p = 0.004$), reward consumption (Figure S3F; two-way ANOVA, group effect: $F_{1,12} = 3$, $p = 0.11$; time effect: $F_{2,24} = 3.8$, $p = 0.04$), or locomotion (Figure S3G; two-way ANOVA, group effect: $F_{1,12} = 0.19$, $p = 0.67$; time effect: $F_{2,24} = 0.26$, $p = 0.77$). Taken together, our optogenetic and chemogenetic manipulations show that, under physiological conditions, PV interneurons selectively promote conditioned behavioral responding in the initial stage of learning when animals are relatively inexperienced. Furthermore, since animals that underwent PV cell suppression recovered to normal performance levels by day 3, it appears that they were still able to learn the stimulus-reward association at the same rate as the control group; however, their ability to express the conditioned response was disrupted early in training.

Learning Diminishes the Relative Influence of PV Interneurons on MSN Activity

Our behavioral data suggest the contribution of PV interneurons relative to other sources of MSN modulation decreases as a function of experience. To probe the learning-dependent influence of PV interneurons on MSN dynamics during behavior, we recorded from two

groups of mice corresponding to the early (day 1; n = 7 $Arch^+$ mice) and late (day 4; n = 7 $Arch^+$ mice) stage of Pavlovian reward conditioning. Using an opto-microprobe, we randomly paired 50% of all CS+ and CS− events with unilateral optical stimulation to suppress the contribution of Arch-expressing PV interneurons on striatal activity (Figure S4A). We found that optical stimulation impacted MSN population activity in a cue-dependent manner, with the change on firing rate during CS+ trials exceeding the change during CS− trials (Figures S4B–S4D; n = 321 MSNs from the day 1 group; Wilcoxon matched pairs signed-rank test, $p < 0.0001$). This demonstrates that striatal PV interneurons contribute more to MSN encoding of reward-associated cues than neutral cues. We also showed that unilateral optical stimulation did not significantly alter anticipatory licking performance in either training group (Figure S4E, paired t-test, day 1: $p = 0.39$; day 4: $p = 0.26$), allowing us to study optogenetically induced changes in neural activity without potentially confounding behavioral changes (Eshel et al., 2015).

Since striatal neurons are known to encode movement-preparatory activity (Fan et al., 2012; Jin and Costa, 2010; Jog et al., 1999; Kimura, 1990; Miyachi et al., 2002; Schultz and Romo, 1992), we examined population activity aligned to the start of an anticipatory licking bout during hit trials. To causally determine the contribution of PV cells to MSN coding, and how their relationship with MSNs changes with learning, we compared population dynamics between light off and light on conditions, and between early (Figures 4A–4C) and late (Figures 4D–4F) stages of training. As a population, MSNs exhibited licking-preparatory activity that increased with time, reaching a maximum level at approximately the lick onset time (Figures 4C, 4F). Transiently suppressing PV cell firing attenuated this activity pattern (Figures 4B, 4C, 4E, 4F). There was an overall reduction in preparatory (see Experimental Procedures; preparatory was defined as t = − 1 to 0 s from lick onset) population activity in both early (Figure 4G; n = 321 MSNs; Wilcoxon matched pairs signed-rank test, $p < 0.0001$) and late (Figure 4H; n = 256 MSNs; Wilcoxon matched pairs signed-rank test, $p < 0.0001$) stages of training, suggesting that PV cells have a persistent role in modulating MSN dynamics. To verify that these effects are optogenetically mediated, we performed measurements in control animals (n = 4 GFP^+ mice) which did not express Arch, and confirmed that there were no light-evoked changes in preparatory MSN dynamics (Figures S4F, S4G; n = 146 MSNs; Wilcoxon matched pairs signed-rank test, $p = 0.93$). We also examined if the change in MSN firing during PV cell suppression was dependent on recording position. We found that the average firing rate change per MSN caused by optical stimulation was not significantly correlated with its position along the dorsal-ventral axis (Figure S5A, day 1: $r = -0.04$, $p = 0.57$; day 4: $r = 0.02$, $p = 0.79$). These results suggest that lick preparatory MSN activity was uniformly affected by optogenetic suppression of PV cells across the depth of the electrode array.

We next examined different aspects of MSN dynamics in animals recorded on day 1 and 4. We found that the absolute amount of light-evoked firing rate suppression remained constant between training days (Figure 4I; Mann-Whitney test, $p = 0.26$). Likewise, the fraction of MSNs that were modulated by the laser did not significantly change (Figure S5B, Mann-Whitney test, $p = 0.073$). We also did not find any significant within-day changes in the firing rate difference between non-laser and laser trials (Figure S5C, one-way ANOVA, day 1: $F_{2,10} = 3.4$, $p = 0.08$; day 4: $F_{2,12} = 0.01$, $p = 0.99$). These results suggest that PV

interneurons alter MSN activity by the same absolute amount independently of the animal's level of training.

On the other hand, we found that MSN firing rate on non-laser trials showed a significant increase from day 1 to 4 (Figure 4J; Mann-Whitney test, $p = 0.026$). There was a concomitant increase in the fraction of significantly excited MSNs (Figure 4K; Mann-Whitney test, $p = 0.002$), and decrease in the fraction of inhibited MSNs (Figure 4L; Mann-Whitney test, $p = 0.019$), indicating that the overall level of preparatory MSN activity increased with training. Since optogenetically suppressing PV cells had the same effect on MSN activity on both training days, but the overall MSN activity was higher, the net effect was that learning diminished the relative suppression of MSNs by PV cells (Figure 4M; Mann-Whitney test, $p = 0.002$).

To further corroborate these findings we examined preparatory FSI activity, which, in contrast to MSNs, did not appear to change with training (Figures 5A, 5B; Mann-Whitney test, $p = 0.38$). We found that neither the fraction of excited (Figure 5C; Mann-Whitney test, $p = 0.25$) nor inhibited (Figure 5D; Mann-Whitney test, $p = 0.25$) FSIs differed between day 1 and day 4 of training. Taken together, these results show that under physiological conditions, striatal MSN activity is enhanced by PV interneurons at all stages of training. However, the contribution of those interneurons relative to other sources of MSN modulation —such as excitatory cortical input—diminishes with experience (Figure 5E). This model is qualitatively consistent with our finding that reward-conditioned behavior was selectively disrupted during the initial phase of training, as this is when preparatory striatal output signals are weakest and therefore most sensitive to attenuation through PV interneuron suppression.

DISCUSSION

PV-expressing interneurons regulate information processing in a wide variety of brain circuits (Hu et al., 2014). Here we found that in the dorsolateral striatum, these cells support reward-conditioned behavioral performance in an experience-dependent manner. We showed that optogenetically or chemogenetically suppressing the activity of these cells selectively interfered with reward-anticipatory licking (hit rate) during the initial stage of learning, but did not affect the performance of experienced animals. Furthermore, the ability to form stimulus-reward associations did not appear to be affected by these manipulations, because after 3 days of training animals reached normal performance levels. These results suggest that DLS PV interneurons are necessary for the initial expression of reward-conditioned responses, but do not control associative learning across different training days. Furthermore, since we showed (by over-activating PV cells to inhibit MSN firing) that the DLS remained necessary for the behavior throughout all stages of training, this suggests that the relative influence of PV cells on DLS microcircuit function declines with experience.

Another study reported dyskinetic behavior upon pharmacological inactivation of FSIs (Gittis et al., 2011b). Here we did not find evidence for deficits in locomotion during suppression of these cells, as measured by cue-evoked rotation of a circular treadmill. On the other hand, activating these cells had a small but significant effect on locomotion. Thus, our

data suggest that PV interneurons are sufficient, but not necessary to drive strong changes in locomotion. The relatively brief optical stimulation used in our study may restrict our ability to detect the onset of dyskinesias. Moreover, a cell ablation study shows that PV-related movement deficits are exacerbated by stress (Xu et al., 2016), which we explicitly tried to reduce in our experiments through gradual habituation to head restraint. Additionally, our study focused on the DLS because PV-positive cells appear to be most concentrated in this area (Luk and Sadikot, 2001), whereas there is evidence that PV cells in other striatal subregions are sufficient to drive different aspects of behavior, such as aversion (Qi et al., 2016). Thus it appears that striatal PV interneurons serve a broader range of functions than the reward conditioning task allowed to be examined here, which may reflect the underlying functional heterogeneity of different striatal subregions (Thorn et al., 2010; van der Meer et al., 2010). For example, PV cells in the dorsomedial striatum (Corbit and Janak, 2010) or nucleus accumbens (Day and Carelli, 2007) may have a stronger role in forming stimulus-reward associations than these interneurons in the DLS, which our data showed regulate the expression of conditioned behaviors. Additionally, striatal PV interneurons appear to represent a molecularly, electrophysiologically, and morphologically diverse population (Koos and Tepper, 1999; Munoz-Manchado et al., 2016), and it is unknown whether these subtypes serve different behavioral functions.

To examine the contribution of PV cells on MSN dynamics, we created an opto-microprobe device by combining silicon-based probe recording technology with optical fibers (Buzsaki et al., 2015). We found that PV cells modulate striatal output signals, and that their contribution to MSN firing rate is the same regardless of the animal's level of experience on the reward conditioning task. In support of this observation, we found no change in preparatory FSI activity during learning. In contrast, learning was accompanied by an increase in preparatory MSN activity from day 1 to 4. The DLS is innervated by glutamatergic afferents from sensorimotor cortical areas (Hintiryan et al., 2016; McGeorge and Faull, 1989; Pennartz et al., 2009). The experience-dependent increase in MSN activity which was observed here, and in other studies (Barnes et al., 2005; Jin and Costa, 2010; Jog et al., 1999; Kimchi et al., 2009; Miyachi et al., 2002; Thorn et al., 2010; Yin et al., 2009), is consistent with an enhancement of corticostriatal coupling that accompanies some forms of learning (Koralek et al., 2013; O'Hare et al., 2016; Xiong et al., 2015). Thus, our results suggest that PV interneurons regulate MSN firing rate by a relatively fixed amount across all stages of training, compared to other inputs whose strength increases as animals gain experience. Finally, some studies show that DLS activity is reduced after extended periods of training (Carelli et al., 1997; Tang et al., 2009), raising the possibility that non-monotonic changes in firing rate may occur after day 4 as animals repeatedly perform the conditioned behavioral response.

In addition to showing that PV interneurons are important for task performance during the initial period of learning, we found complementary behavioral and electrophysiological evidence that these cells play a role unlike their counterparts in cortical microcircuits. Namely, both PV cell hypoactivity and hyperactivity reduced reward conditioning and spontaneous MSN output. The PV inactivation experiments demonstrate that under physiological conditions, striatal PV interneurons amplify MSN activity, and that this enhances the expression of anticipatory lick responses. Conversely, the over-activation

experiments demonstrate that PV interneurons are sufficient to disrupt neural dynamics and behavior. An open question is the biological significance of these results. Suppression of activity (reduction of function) may mimic the acute effects of a sparser PV cell population, which is associated with disorders such as Tourette syndrome (Kalanithi et al., 2005) and Huntington's disease (Reiner et al., 2013). In contrast, manipulations to excessively drive these cells do not reflect any known physiological state, but are nevertheless useful for inhibiting DLS output signals and assessing their sufficiency in driving behavior.

The most extensively studied connection of striatal PV interneurons is monosynaptic coupling with MSNs (Gittis et al., 2010; Koos and Tepper, 1999; Mallet et al., 2005; Planert et al., 2010; Tepper et al., 2010). However, our data also showed the presence of disynaptic inhibitory coupling via an intermediary interneuron. Using *in vitro* electrophysiology we identified an inhibitory connection from PV to NPY interneurons, which preferentially occurred in the NGF rather than the PLTS subpopulation. Moreover, we confirmed that activation of NPY interneurons potently reduced MSN activity *in vivo*, in agreement with previously reported findings in brain slices (English et al., 2012; Ibanez-Sandoval et al., 2011). Thus we identified a possible mechanism by which suppressing PV interneurons inhibits MSN firing, via disinhibition of NPY interneurons. It is notable that NPY-NGF cells may provide even stronger inhibition to MSNs than PV interneurons (Ibanez-Sandoval et al., 2011), which supports our proposed mechanism. Conversely, we speculate that excessively activating PV interneurons causes monosynaptic inhibition onto MSNs to override disynaptic disinhibition, again resulting in net MSN inhibition. A full understanding of the implications of these competing inhibitory coupling mechanisms requires further study, but they may have evolved to enable specialized computations in striatal microcircuits, such as detecting the absolute value of changes in PV cell firing.

In addition to the disynaptic PV-NPY-MSN circuit, we note other mechanisms that may contribute to some of our observations. It is known that the chloride reversal potential can lead to GABA-mediated depolarization on MSNs under certain conditions (Berke, 2011; Bracci and Panzeri, 2006; Czubayko and Plenz, 2002; Humphries et al., 2009; Plenz, 2003). However, this effect appears to be confined to MSNs below the chloride reversal potential, whereas neurons above the reversal potential are hyperpolarized by GABA (Plenz, 2003). Thus, it is unclear how to reconcile GABA-mediated depolarization with all of our results, in which MSN activity was attenuated by PV interneuron suppression under conditions of both low (spontaneous) and elevated (task-evoked) firing. Furthermore, it has been proposed that NPY-NGF interneurons can inhibit glutamate release from corticostriatal terminals through $GABA_B$ receptors (Logie et al., 2013). If, as we propose, NPY-NGF interneurons get disinhibited by PV interneuron silencing, glutamate released from corticostriatal terminals would be reduced, making it less likely for MSNs to generate action potentials. It is also possible that disynaptic coupling via MSNs (PV-MSN-MSN interactions) may contribute, in light of work showing the importance of lateral inhibition in regulating striatal output (Dobbs et al., 2016; Planert et al., 2010; Plenz, 2003). In addition to local microcircuit mechanisms, the inhibitory effect of PV interneuron suppression on MSN firing may be mediated by negative feedback with cortical areas projecting to the DLS. This could arise if there is a significant bias in the connectivity of PV cells toward direct pathway MSNs, as suggested by some studies (Gittis et al., 2011a; Gittis et al., 2010). To examine this possible

mechanism, we tested whether suppressing striatal PV interneurons has any effect on the spontaneous firing of the secondary motor cortex. We found no significant change in the mean pyramidal cell firing rate, which does not appear to support the long-range negative feedback mechanism with this specific cortical region. However, this does not rule out the possibility that other brain areas provide negative feedback to the DLS during PV interneuron suppression. Thus, while the competition between monosynaptic (PV-MSN) and disynaptic (PV-NPY-MSN) inhibition provides a parsimonious explanation for the results of our optogenetic suppression and over-activation experiments, there may be synergistic effects with other local and long-range circuit mechanisms, such as those noted above.

We showed that under physiological conditions, PV interneurons increase MSN activity to enhance behavioral performance in a reward conditioning task. As learning progresses, the contribution of PV cells relative to other sources of MSN input declines, together with their involvement in behavior. These results suggest that the abnormal function of PV cells, which is linked to a number of neurological disorders (Cepeda et al., 2013; Gittis et al., 2011a; Kalanithi et al., 2005; Mallet et al., 2006; Reiner et al., 2013), may cause the most severe behavioral deficits in the early stages of striatal-dependent learning. These findings also may provide new insights for probing the function of interneurons in learning and behavior.

METHODS

CONTACT FOR REAGENT AND RESOURCE SHARING

Further information and requests for resources, reagents, data, and custom software scripts should be directed to and will be fulfilled by the Lead Contact (smasmanidis@ucla.edu).

EXPERIMENTAL MODEL AND SUBJECT DETAILS

Homozygous PV-Cre mice (Hippenmeyer et al., 2005) (Pvalb$^{tm1(cre)Arbr}$, The Jackson Laboratory), of either sex, 8–12 weeks were used for *in vivo* PV interneuron manipulations. BAC transgenic NPY-Cre mice (Tg(Npy-cre)RH26Gsat/Mmucd, Mutant Mouse Resource and Research Centers) bred with C57BL/6J mice were used for *in vivo* NPY interneuron manipulations. For *in vitro* experiments we crossed hemizygous NPY-GFP mice (B6.FVB-Tg(Npy-hrGFP)1Lowl/J) (van den Pol et al., 2009) with homozygous PV-Cre mice. Genotyping was carried out on tail samples (Transnetyx). Animals were group housed until the surgery. Animals were kept on a 12 hr light cycle. All procedures were approved by the University of California, Los Angeles Chancellor's Animal Research Committee.

METHOD DETAILS

Surgeries and viral injections—Animals underwent a surgical procedure under aseptic conditions and isoflurane anesthesia on a stereotaxic apparatus. We injected carprofen (5 mg/kg, s.c.) daily for the first three days post-operatively. We attached rectangular head fixation bars on each side of the skull (9 mm × 7 mm × 0.76 mm dimensions, 0.6 g weight, laser cut from stainless steel at Fab2Order). Cre-dependent adeno-associated virus (AAV) was obtained from the University of North Carolina Vector Core. Using pulled glass pipettes we injected either AAV5/Flex-ARCH-GFP, AAV5/Syn-Flex-ChrimsonR-tdTomato, AAV5/EF1a-DIO-eNpHR3.0-eYFP, or AAV5/EF1a-DIO-hChR2(H134R)-EYFP (for *in vitro*

experiments), AAV5/Flex-GFP (for control experiments), or AAV8/hSyn-DIO-hm4D(Gi)-mcherry (for chemogenetic experiments), unilaterally or bilaterally into the dorsolateral striatum (500 nl per hemisphere, 0.8 mm anterior, 2.2 mm lateral, 3.2 mm ventral to bregma). In another set of experiments we injected AAV5/Flex-ARCH-GFP into the medial prefrontal cortex (300 nl, 1.8 mm anterior, 0.25 mm lateral, 2.5 mm ventral to bregma). For behavioral manipulation experiments we also bilaterally implanted ferrule-coupled optical fibers (200 μm diameter, 0.22 NA) that terminated 200 μm above the striatal injection sites. All animals were individually housed after surgery, and were allowed to recover for 2 weeks before beginning habituation and behavioral conditioning (see Behavioral task). Analgesics (ibuprofen) and antibiotics (amoxicillin) were administered in the drinking water for the first week post-operatively. For electrophysiological experiments, a second surgery under isoflurane anesthesia was completed 6 hrs prior to recording, to create a rectangular craniotomy above the region of interest. A drop of bupivacaine was applied on the skull before drilling craniotomies. An additional craniotomy was made over the posterior cerebellum to accommodate a silver/silver-chloride electrical reference wire.

Immunohistochemistry—Brain sections from n=4 $Arch^+$ mice were immunostained with antibodies to PV and GFP to visualize Arch expression, and NeuN to visualize neuronal nuclei. PV-Cre mice injected with AAV5/Flex-Arch-GFP were perfused with 24 °C phosphate-buffered saline (pH 7.3) and ice-cold paraformaldehyde. Brains were placed in paraformaldehyde overnight, and were cut as coronal sections with a thickness of 100 μm on a vibratome. Subsequently, goat antibody to PV (1:1,000, SWant), rabbit antibody to NeuN (1:1000, Millipore) and chicken antibody to GFP (1:1,000, Abcam) primary antibodies were used, followed by Alexa Fluor 647-conjugated donkey antibody to goat (1:200, Jackson ImmunoResearch) and DyLight 405–conjugated donkey antibody to rabbit (1:200, Jackson ImmunoResearch) and Alexa Fluor 488–conjugated donkey antibody to chicken (1:200, Jackson ImmunoResearch) as secondary antibodies. Sections were imaged under confocal microscopy, and cells were counted manually. The quantification of GFP and PV expression levels is provided in Figure S1B.

Behavioral task—After 2 weeks of recovery from the first surgery, mice were food restricted to maintain their weight at around 90% of their baseline level, and given water *ad libitum*. Habituation and training procedures are described in detail in another publication (Shobe et al., 2015). The timeline is illustrated in Figure S3B. Briefly, animals were initially habituated to the head fixation apparatus and to reliably consume uncued rewards (5 μl, 10% sweetened condensed milk), which were delivered via actuation of an audible solenoid valve. The reward delivery and lick meter port was located around 5 mm from the mouth, and animals had to extend their tongue out of the mouth to register as a lick. Subsequently, animals were trained on a Pavlovian task using olfactory cues. Aromatic compounds (isoamyl acetate for CS+, and citral for CS−) were diluted 1:10 in mineral oil, and diluted another factor of 10 by mixing with clean air in an olfactometer (total air flow was 1.5 l/min). For experiments involving optogenetic manipulations, cues were presented in pseudorandom order for 1 s, followed by a reward 3 s after CS+ onset (100 CS+ and 100 CS − cues per session, 15–25 s intertrial interval). Hit rate for optogenetic experiments was defined as the fraction of CS+ trials with a bout of licking starting 0–3 s after CS+ onset

(*i.e.*, prior to reward delivery). For experiments involving chemogenetic manipulations, cues were presented in pseudorandom order for 1 s, followed by a reward 2.5 s after CS+ onset (100 CS+ and 100 CS− cues per session, 15–25 s intertrial interval). Hit rate for chemogenetic experiments was defined as the fraction of CS+ trials with a bout of licking starting 0–2.5 s after CS+ onset (*i.e.*, prior to reward delivery). False alarm rate for all experiments was defined as the fraction of CS− trials with licking 0–5 s after CS− onset. Consumption rate for all experiments was defined as the fraction of rewards in which animals licked 0–0.5 s after reward onset. Treadmill speed was calculated as the mean rotational velocity in a 5 s period after cue offset, averaged across all CS+ trials.

***In vivo* optical stimulation and chemogenetics—**Optical stimulation was provided through a pair of optical fibers. The fibers were coupled to a laser (Opto Engine) through a 50/50 splitter (532 nm, 10 mW per fiber unless the power was explicitly varied). In the first optogenetic behavioral cohort (Figures 3A–3D, S3C, S3D) light was delivered throughout 3 days of training in previously inexperienced animals, between 1–6 s after cue onset. In the second optogenetic behavioral cohort (Figures 3E, S3E), mice were initially trained for 3 days without optical stimulation. On the 4th day mice were presented with 40 CS+ and 40 CS− trials without light (“Pre”), an equal number of trials with light (“Laser”, same stimulation parameters as the first cohort), and again an equal number of trials without light (“Post”). In the chemogenetic behavioral cohort (Figures 3F, 3G, S3F, S3G), we injected CNO (1 mg/kg, 150 μl, i.p.) or vehicle (150 μl, i.p.) 45 min before beginning training for 3 days of training in previously inexperienced animals. In electrophysiological experiments involving spontaneous firing rate measurements (Figures 1, 2E, S1–S3), light was delivered in 5 s continuous pulses in the absence of any explicit cues or rewards. Light intensity was varied from 1, 2, 5, 10, 15 mW (20 trials per setting). In electrophysiological experiments involving behavioral training (Figures 4, 5, S4–S5), light (10 mW) was delivered on 50% of all CS+ and CS− trials, from 1 to 6 s after cue onset.

Opto-microprobe and *in vivo* electrophysiology—The device used to concurrently record neural activity and optically suppress PV cells consisted of a 256 electrode silicon microprobe (Shobe et al., 2015) (4 prongs spaced by 200 μm, 64 electrodes per prong in a honeycomb array pattern spanning 1.05 mm), integrated with a pair of optical fibers (200 μm diameter, 0.22 NA) with their centers spaced 400 μm apart. Electrode impedance was set to 100–300 kΩ via gold electrodeposition. The device was cleaned after each recording session in a trypsin solution and deionized water, and reused in subsequent experiments. Optical intensity from each fiber was calibrated prior to every recording, and measured again at the end of the recording to ensure stability. On the recording day, animals underwent a brief craniotomy surgery under isoflurane anesthesia. The dura was removed to facilitate insertion. During a 6 hr recovery period, the craniotomies were sealed with a silicone elastomer compound (Kwik-Cast, World Precision Instruments). Subsequently, awake animals were head restrained, the elastomer was removed from the craniotomies, the reference wire was placed on the surface of the cerebellum, and the opto-microprobe was inserted in the brain under the control of a motorized micromanipulator. For recordings in the dorsolateral striatum, the target coordinates of the most lateral silicon prong were: 0.8 mm anterior, 2.5 mm lateral, 4.2 mm ventral to bregma. For recordings in the prefrontal

cortex, the target coordinates of the most lateral prong were: 1.8 mm anterior, 0.7 mm lateral, 3.0 mm ventral to bregma. For recordings in the motor cortex, the target coordinates of the most lateral prong were: 2.4 mm anterior, 1.8 mm lateral, 2.1 mm ventral to bregma. Mineral oil was placed on the craniotomy to prevent drying. Data acquisition commenced 45 min after device insertion, using custom-built hardware at a sampling rate of 25 kHz per electrode (Shobe et al., 2015).

***In vitro* electrophysiology—**Recordings were performed in brain slices from 12 week-old PV-Cre × NPY-GFP mice at 4–5 weeks following AAV injection. To prepare brain slices, mice were deeply anesthetized with isoflurane and perfused transcardially with an ice-cold, high sucrose-based slicing solution containing (in mM): 26 $NaHCO_3$, 1.25 NaH_2PO_4, 208 sucrose, 10 glucose, 2.5 KCl, 1.3 $MgCl_2$, 8 $MgSO_4$. Mice were decapitated, brains dissected out and immediately placed in oxygenated sucrose slicing solution. Coronal slices (300 μm) were cut and transferred to an incubating chamber containing ACSF (in mM): 130 NaCl, 3 KCl, 1.25 NaH_2PO_4, 26 $NaHCO_3$, 2 $MgCl_2$, 2 $CaCl_2$, and 10 glucose) oxygenated with 95% O_2-5% CO_2 (pH 7.2–7.4, osmolality 290–310 mOsm/L, 32–34°C). Slices were al lowed to recover for an additional 30 min at room temperature prior to recording. All recordings were performed at room temperature using an upright microscope (Olympus BX51WI) equipped with differential interference contrast optics and fluorescence imaging (QIACAM fast 1394 monochromatic camera with Q-Capture Pro software, Qlmaging). Whole-cell patch clamp recordings in voltage and current-clamp modes were obtained from GFP-positive NPY cells using a MultiClamp 700B Amplifier (Molecular Devices) and the pCLAMP 10.3 acquisition software. The patch pipette (3–5 MΩ resistance) contained a cesium-based internal solution (in mM): 125 Cs-methanesulfonate, 4 NaCl, 1 $MgCl_2$, 5 MgATP, 9 EGTA, 8 HEPES, 1 GTP-Tris, 10 phosphocreatine, and 0.1 leupeptin (pH 7.2 with CsOH, 270–280 mOsm) for voltage-clamp recordings or a K-gluconate-based solution containing (in mM): 112.5 K-gluconate, 4 NaCl, 17.5 KCl, 0.5 $CaCl_2$, 1 $MgCl_2$, 5 ATP (potassium salt), 1 NaGTP, 5 EGTA, 10 HEPES, pH 7.2 (270–280 mOsm/L) for current-clamp recordings. After breaking through the membrane, cell properties (capacitance, input resistance, decay time constant) were recorded while holding the membrane potential at −70 mV. Electrode access resistances during whole-cell recordings were maintained at < 30 MΩ. PV interneurons were activated with a single light pulse (470 nm, 0.5 ms, 3 mW, CoolLED) delivered through the epifluorescence illumination pathway using Chroma Technologies filter cubes. Evoked IPSCs in response to optical activation were recorded in MSNs and NPY-GFP cells in voltage-clamp mode, at a holding potential of +10 mV and in the presence of glutamatergic receptor antagonists (10 μM NBQX and 50 μM APV, Tocris Bioscience). In some cells, 20 μM bicuculline was applied to block optically evoked IPSC responses, confirming their GABAergic nature.

Data analysis—Spike sorting and all neural activity analysis was carried out with custom Matlab scripts. Striatal units were classified using previously described criteria (Bakhurin et al., 2016) as putative medium spiny neurons (MSNs), fast spiking interneurons (FSIs), or tonically active neurons (TANs), based on spike waveform peak-to-trough width, and coefficient of variation of the baseline firing rate. There is no established procedure for electrophysiologically identifying putative NPY NGF or PLTS cells *in vivo.* FSIs were

characterized by a narrow spike waveform (maximum width = 0.475 ms, Figure 1C). MSNs and TANs both have wider waveforms (minimum width = 0.55 ms, maximum width = 1.25 ms). TANs were separated from MSNs by the regularity of their baseline firing (maximum coefficient of variation = 1.5). Units in the prefrontal cortex were classified as putative FSIs or pyramidal neurons using the same spike width separation criterion described for striatal FSIs. Firing rate was calculated by convolving spike times with a Gaussian filter (SD = 50 ms) in time steps of 10 ms.

To calculate the change in spontaneous firing rate and rate modulation index during optical stimulation, we took into account that some units, regardless of whether animals were injected with optogenetic constructs, showed a transient increase in activity at the onset of the light stimulus (Figure 1G). This suggests the presence of a visual response artifact to green light, which has also been reported elsewhere (Kravitz et al., 2013), despite our best attempt to shield light from the animal's eyes. Since this artifact appears confined to the onset of illumination, we excluded the first 1 s post-laser onset in the calculation of spontaneous activity effects. The change in spontaneous firing rate was calculated as the mean difference in rate between 1–5 s post-laser onset, and 0–1 s pre-laser onset (*i.e.*, the baseline period). The rate modulation index per unit (RMI) was defined by the expression:

$$\mathrm{RMI}=(\mathrm{R}_2-\mathrm{R}_1)/(\mathrm{R}_1+\mathrm{R}_2) \quad (1)$$

where R_2 represents the mean firing 1–5 s post-laser onset, and R_1 represents the mean baseline firing rate 0–1 s pre-laser onset. The RMI is a unitless quantity from −1 to 1, with negative values indicating net suppression of activity relative to baseline, and positive values indicating net excitation.

To compare neural population activity between laser-off and laser-on conditions, we aligned the firing rate to the onset of the first lick, and averaged over all hit trials. We then pooled units from all animals, and applied a paired t-test to calculate the likelihood, at each time bin, that the population activity from the laser-off and laser-on trials was indistinguishable.

To determine the licking-evoked firing rate change per animal for each unit, we calculated the difference in mean firing rate between the lick preparatory period (defined as t = −1 to 0 s from lick onset), and a baseline period (defined as t = −7 to −3 s from lick onset). We then plotted the median rate change of all selected units per animal, and compared distributions across the day 1 and 4 groups. To obtain the fraction of excited and inhibited units, we randomly permuted each time bin of the firing rate in the lick preparatory period (t = −1 to 0 s) with the baseline period (t=−7 to −3 s), and calculated the permuted firing rate change (500 iterations). We then calculated the likelihood that the observed rate change at a particular time bin was equal to the permuted rate change. The significance criterion was defined as $p < 0.01$. If two or more consecutive time bins had a significant positive (negative) change, that unit was defined as excited (inhibited). To obtain the fraction of laser-modulated units, we randomly swapped activity between non-laser and laser trials for each time bin in the lick preparatory period. We then calculated the likelihood that the observed difference in firing rate between non-laser and laser trials at a particular time bin

was greater than the permuted difference. If two or more consecutive time bins significantly discriminated between non-laser and laser trials, that unit was defined as laser-modulated.

To determine the absolute amount of MSN firing rate suppression mediated by suppressing PV interneurons (Figure 4I), we calculated the following expression:

$$\text{Firing rate suppression} = R_{off} - R_{on} \quad (2)$$

where R_{off} (R_{on}) is the median firing rate of all MSNs per animal in the lick preparatory period (t = −1 to 0 s) on hit trials with laser off (on). To determine the amount of MSN firing rate suppression relative to the total MSN rate (Figure 4M), we used the following expression:

$$\text{Relative suppression} = 1 - (\Delta R_{off} - \Delta R_{on})/(\Delta R_{off} + \Delta R_{on}) \quad (3)$$

where ΔR_{off} (ΔR_{on}) is the median firing rate change of all MSNs per animal between the lick preparatory period (t = −1 to 0 s) and baseline period (t = −7 to −3 s), on hit trials with laser off (on). The relative suppression factor is a unitless quantity, with smaller values reflecting a smaller effect of suppressing PV cells on MSN activity relative to the overall MSN activity.

QUANTIFICATION AND STATISTICAL ANALYSIS

All statistical analyses were performed using standard Matlab functions, custom scripts, or Prism software. One-way analysis of variance (ANOVA) was accompanied by Tukey's *post hoc* test for multiple comparisons. Two-way ANOVA was accompanied by Bonferroni's *post hoc* test for multiple comparisons. The difference between day 1 and day 4 group neural activity was evaluated by a Mann-Whitney U test. The sign of the rate modulation index (RMI) was determined by a Wilcoxon signed-rank test for zero median. We excluded one animal from the results in Figure S5C, because the mouse did not perform enough correct anticipatory licking trials to be included in the within-session activity analysis. Information about the exact value of n, what n represents, statistical test used, p-value, and use of SD or SEM is provided in the main text and/or figure captions. Statistical results are summarized in Table S1.

Supplementary Material

Refer to Web version on PubMed Central for supplementary material.

Acknowledgments

We thank E.S. Boyden and K. Deisseroth for sharing optogenetic constructs and B.L. Roth for sharing DREADD constructs used in this project, which were obtained from the University of North Carolina Vector Core. S.C.M. acknowledges support from a 2014 McKnight Technical Innovations in Neuroscience Award, NIH DA034178, NIH NS100050, and NSF CBET 1263785. M.S.L. acknowledges support from NIH NS41574, and NIH U54HD087101, which supports the Cell, Circuits and Systems Analysis Core.

References

Armbruster BN, Li X, Pausch MH, Herlitze S, Roth BL. Evolving the lock to fit the key to create a family of G protein-coupled receptors potently activated by an inert ligand. Proc Natl Acad Sci U S A. 2007; 104:5163–5168. [PubMed: 17360345]

Bakhurin KI, Mac V, Golshani P, Masmanidis SC. Temporal correlations among functionally specialized striatal neural ensembles in reward-conditioned mice. J Neurophysiol. 2016; 115:1521–1532. [PubMed: 26763779]

Balleine BW, Delgado MR, Hikosaka O. The role of the dorsal striatum in reward and decision-making. J Neurosci. 2007; 27:8161–8165. [PubMed: 17670959]

Barbera G, Liang B, Zhang L, Gerfen CR, Culurciello E, Chen R, Li Y, Lin DT. Spatially Compact Neural Clusters in the Dorsal Striatum Encode Locomotion Relevant Information. Neuron. 2016

Barnes TD, Kubota Y, Hu D, Jin DZ, Graybiel AM. Activity of striatal neurons reflects dynamic encoding and recoding of procedural memories. Nature. 2005; 437:1158–1161. [PubMed: 16237445]

Bennett BD, Wilson CJ. Spontaneous activity of neostriatal cholinergic interneurons in vitro. J Neurosci. 1999; 19:5586–5596. [PubMed: 10377365]

Berke JD. Functional properties of striatal fast-spiking interneurons. Front Syst Neurosci. 2011; 5:45. [PubMed: 21743805]

Bracci E, Panzeri S. Excitatory GABAergic effects in striatal projection neurons. J Neurophysiol. 2006; 95:1285–1290. [PubMed: 16251264]

Burguiere E, Monteiro P, Feng G, Graybiel AM. Optogenetic stimulation of lateral orbitofronto-striatal pathway suppresses compulsive behaviors. Science. 2013; 340:1243–1246. [PubMed: 23744950]

Buzsaki G, Stark E, Berenyi A, Khodagholy D, Kipke DR, Yoon E, Wise KD. Tools for probing local circuits: high-density silicon probes combined with optogenetics. Neuron. 2015; 86:92–105. [PubMed: 25856489]

Carelli RM, Wolske M, West MO. Loss of lever press-related firing of rat striatal forelimb neurons after repeated sessions in a lever pressing task. J Neurosci. 1997; 17:1804–1814. [PubMed: 9030639]

Cepeda C, Galvan L, Holley SM, Rao SP, Andre VM, Botelho EP, Chen JY, Watson JB, Deisseroth K, Levine MS. Multiple sources of striatal inhibition are differentially affected in Huntington's disease mouse models. J Neurosci. 2013; 33:7393–7406. [PubMed: 23616545]

Chow BY, Han X, Dobry AS, Qian X, Chuong AS, Li M, Henninger MA, Belfort GM, Lin Y, Monahan PE, Boyden ES. High-performance genetically targetable optical neural silencing by light-driven proton pumps. Nature. 2010; 463:98–102. [PubMed: 20054397]

Cohen JY, Haesler S, Vong L, Lowell BB, Uchida N. Neuron-type-specific signals for reward and punishment in the ventral tegmental area. Nature. 2012; 482:85–88. [PubMed: 22258508]

Corbit LH, Janak PH. Inactivation of the lateral but not medial dorsal striatum eliminates the excitatory impact of Pavlovian stimuli on instrumental responding. J Neurosci. 2007; 27:13977–13981. [PubMed: 18094235]

Corbit LH, Janak PH. Posterior dorsomedial striatum is critical for both selective instrumental and Pavlovian reward learning. Eur J Neurosci. 2010; 31:1312–1321. [PubMed: 20345912]

Cui G, Jun SB, Jin X, Pham MD, Vogel SS, Lovinger DM, Costa RM. Concurrent activation of striatal direct and indirect pathways during action initiation. Nature. 2013; 494:238–242. [PubMed: 23354054]

Czubayko U, Plenz D. Fast synaptic transmission between striatal spiny projection neurons. Proc Natl Acad Sci U S A. 2002; 99:15764–15769. [PubMed: 12438690]

Damodaran S, Evans RC, Blackwell KT. Synchronized firing of fast-spiking interneurons is critical to maintain balanced firing between direct and indirect pathway neurons of the striatum. J Neurophysiol. 2014; 111:836–848. [PubMed: 24304860]

Day JJ, Carelli RM. The nucleus accumbens and Pavlovian reward learning. The Neuroscientist: a review journal bringing neurobiology, neurology and psychiatry. 2007; 13:148–159.

Dobbs LK, Kaplan AR, Lemos JC, Matsui A, Rubinstein M, Alvarez VA. Dopamine Regulation of Lateral Inhibition between Striatal Neurons Gates the Stimulant Actions of Cocaine. Neuron. 2016; 90:1100–1113. [PubMed: 27181061]

English DF, Ibanez-Sandoval O, Stark E, Tecuapetla F, Buzsaki G, Deisseroth K, Tepper JM, Koos T. GABAergic circuits mediate the reinforcement-related signals of striatal cholinergic interneurons. Nat Neurosci. 2012; 15:123–130.

Eshel N, Bukwich M, Rao V, Hemmelder V, Tian J, Uchida N. Arithmetic and local circuitry underlying dopamine prediction errors. Nature. 2015

Fan D, Rossi MA, Yin HH. Mechanisms of action selection and timing in substantia nigra neurons. J Neurosci. 2012; 32:5534–5548. [PubMed: 22514315]

Fanselow MS, Wassum KM. The Origins and Organization of Vertebrate Pavlovian Conditioning. Cold Spring Harbor perspectives in biology. 2015; 8

Fino E, Venance L. Spike-timing dependent plasticity in striatal interneurons. Neuropharmacology. 2011; 60:780–788. [PubMed: 21262240]

Gage GJ, Stoetzner CR, Wiltschko AB, Berke JD. Selective activation of striatal fast-spiking interneurons during choice execution. Neuron. 2010; 67:466–479. [PubMed: 20696383]

Gerfen CR, Surmeier DJ. Modulation of striatal projection systems by dopamine. Annu Rev Neurosci. 2011; 34:441–466. [PubMed: 21469956]

Gittis AH, Hang GB, LaDow ES, Shoenfeld LR, Atallah BV, Finkbeiner S, Kreitzer AC. Rapid target-specific remodeling of fast-spiking inhibitory circuits after loss of dopamine. Neuron. 2011a; 71:858–868. [PubMed: 21903079]

Gittis AH, Leventhal DK, Fensterheim BA, Pettibone JR, Berke JD, Kreitzer AC. Selective inhibition of striatal fast-spiking interneurons causes dyskinesias. J Neurosci. 2011b; 31:15727–15731. [PubMed: 22049415]

Gittis AH, Nelson AB, Thwin MT, Palop JJ, Kreitzer AC. Distinct roles of GABAergic interneurons in the regulation of striatal output pathways. J Neurosci. 2010; 30:2223–2234. [PubMed: 20147549]

Gradinaru V, Thompson KR, Deisseroth K. eNpHR: a Natronomonas halorhodopsin enhanced for optogenetic applications. Brain cell biology. 2008; 36:129–139. [PubMed: 18677566]

Graybiel AM. Habits, rituals, and the evaluative brain. Annu Rev Neurosci. 2008; 31:359–387. [PubMed: 18558860]

Graybiel AM, Grafton ST. The Striatum: Where Skills and Habits Meet. Cold Spring Harbor perspectives in biology. 2015; 7

Han JS, McMahan RW, Holland P, Gallagher M. The role of an amygdalo-nigrostriatal pathway in associative learning. J Neurosci. 1997; 17:3913–3919. [PubMed: 9133409]

Hintiryan H, Foster NN, Bowman I, Bay M, Song MY, Gou L, Yamashita S, Bienkowski MS, Zingg B, Zhu M, et al. The mouse cortico-striatal projectome. Nat Neurosci. 2016; 19:1100–1114. [PubMed: 27322419]

Hippenmeyer S, Vrieseling E, Sigrist M, Portmann T, Laengle C, Ladle DR, Arber S. A developmental switch in the response of DRG neurons to ETS transcription factor signaling. PLoS biology. 2005; 3:e159. [PubMed: 15836427]

Hjorth J, Blackwell KT, Kotaleski JH. Gap junctions between striatal fast-spiking interneurons regulate spiking activity and synchronization as a function of cortical activity. J Neurosci. 2009; 29:5276–5286. [PubMed: 19386924]

Hu H, Gan J, Jonas P. Interneurons. Fast-spiking, parvalbumin(+) GABAergic interneurons: from cellular design to microcircuit function. Science. 2014; 345:1255263. [PubMed: 25082707]

Humphries MD, Wood R, Gurney K. Dopamine-modulated dynamic cell assemblies generated by the GABAergic striatal microcircuit. Neural networks: the official journal of the International Neural Network Society. 2009; 22:1174–1188. [PubMed: 19646846]

Ibanez-Sandoval O, Tecuapetla F, Unal B, Shah F, Koos T, Tepper JM. A novel functionally distinct subtype of striatal neuropeptide Y interneuron. J Neurosci. 2011; 31:16757–16769. [PubMed: 22090502]

Jin X, Costa RM. Start/stop signals emerge in nigrostriatal circuits during sequence learning. Nature. 2010; 466:457–462. [PubMed: 20651684]

Jog MS, Kubota Y, Connolly CI, Hillegaart V, Graybiel AM. Building neural representations of habits. Science. 1999; 286:1745–1749. [PubMed: 10576743]

Kalanithi PS, Zheng W, Kataoka Y, DiFiglia M, Grantz H, Saper CB, Schwartz ML, Leckman JF, Vaccarino FM. Altered parvalbumin-positive neuron distribution in basal ganglia of individuals with Tourette syndrome. Proc Natl Acad Sci U S A. 2005; 102:13307–13312. [PubMed: 16131542]

Kimchi EY, Torregrossa MM, Taylor JR, Laubach M. Neuronal correlates of instrumental learning in the dorsal striatum. J Neurophysiol. 2009; 102:475–489. [PubMed: 19439679]

Kimura M. Behaviorally contingent property of movement-related activity of the primate putamen. J Neurophysiol. 1990; 63:1277–1296. [PubMed: 2358877]

Kita H, Kosaka T, Heizmann CW. Parvalbumin-immunoreactive neurons in the rat neostriatum: a light and electron microscopic study. Brain Res. 1990; 536:1–15. [PubMed: 2085740]

Klapoetke NC, Murata Y, Kim SS, Pulver SR, Birdsey-Benson A, Cho YK, Morimoto TK, Chuong AS, Carpenter EJ, Tian Z, et al. Independent optical excitation of distinct neural populations. Nature methods. 2014; 11:338–346. [PubMed: 24509633]

Koos T, Tepper JM. Inhibitory control of neostriatal projection neurons by GABAergic interneurons. Nat Neurosci. 1999; 2:467–472. [PubMed: 10321252]

Koralek AC, Costa RM, Carmena JM. Temporally precise cell-specific coherence develops in corticostriatal networks during learning. Neuron. 2013; 79:865–872. [PubMed: 23954030]

Kravitz AV, Freeze BS, Parker PR, Kay K, Thwin MT, Deisseroth K, Kreitzer AC. Regulation of parkinsonian motor behaviours by optogenetic control of basal ganglia circuitry. Nature. 2010; 466:622–626. [PubMed: 20613723]

Kravitz AV, Owen SF, Kreitzer AC. Optogenetic identification of striatal projection neuron subtypes during in vivo recordings. Brain Res. 2013; 1511:21–32. [PubMed: 23178332]

Kravitz AV, Tye LD, Kreitzer AC. Distinct roles for direct and indirect pathway striatal neurons in reinforcement. Nat Neurosci. 2012; 15:816–818. [PubMed: 22544310]

Kreitzer AC, Malenka RC. Striatal plasticity and basal ganglia circuit function. Neuron. 2008; 60:543–554. [PubMed: 19038213]

Lau T, Gage GJ, Berke JD, Zochowski M. Local dynamics of gap-junction-coupled interneuron networks. Physical biology. 2010; 7:16015. [PubMed: 20228446]

Liljeholm M, O'Doherty JP. Contributions of the striatum to learning, motivation, and performance: an associative account. Trends in cognitive sciences. 2012; 16:467–475. [PubMed: 22890090]

Logie C, Bagetta V, Bracci E. Presynaptic control of corticostriatal synapses by endogenous gaba. J Neurosci. 2013; 33:15425–15431. [PubMed: 24068811]

Luk KC, Sadikot AF. GABA promotes survival but not proliferation of parvalbumin-immunoreactive interneurons in rodent neostriatum: an in vivo study with stereology. Neuroscience. 2001; 104:93–103. [PubMed: 11311534]

Mahn M, Prigge M, Ron S, Levy R, Yizhar O. Biophysical constraints of optogenetic inhibition at presynaptic terminals. Nat Neurosci. 2016; 19:554–556. [PubMed: 26950004]

Mallet N, Ballion B, Le Moine C, Gonon F. Cortical inputs and GABA interneurons imbalance projection neurons in the striatum of parkinsonian rats. J Neurosci. 2006; 26:3875–3884. [PubMed: 16597742]

Mallet N, Le Moine C, Charpier S, Gonon F. Feedforward inhibition of projection neurons by fast-spiking GABA interneurons in the rat striatum in vivo. J Neurosci. 2005; 25:3857–3869. [PubMed: 15829638]

McGeorge AJ, Faull RL. The organization of the projection from the cerebral cortex to the striatum in the rat. Neuroscience. 1989; 29:503–537. [PubMed: 2472578]

Miyachi S, Hikosaka O, Lu X. Differential activation of monkey striatal neurons in the early and late stages of procedural learning. Exp Brain Res. 2002; 146:122–126. [PubMed: 12192586]

Moyer JT, Halterman BL, Finkel LH, Wolf JA. Lateral and feedforward inhibition suppress asynchronous activity in a large, biophysically-detailed computational model of the striatal network. Frontiers in computational neuroscience. 2014; 8:152. [PubMed: 25505406]

Munoz-Manchado AB, Foldi C, Szydlowski S, Sjulson L, Farries M, Wilson C, Silberberg G, Hjerling-Leffler J. Novel Striatal GABAergic Interneuron Populations Labeled in the 5HT3a(EGFP) Mouse. Cereb Cortex. 2016; 26:96–105. [PubMed: 25146369]

Nelson AB, Hammack N, Yang CF, Shah NM, Seal RP, Kreitzer AC. Striatal cholinergic interneurons Drive GABA release from dopamine terminals. Neuron. 2014; 82:63–70. [PubMed: 24613418]

O'Hare JK, Ade KK, Sukharnikova T, Van Hooser SD, Palmeri ML, Yin HH, Calakos N. Pathway-Specific Striatal Substrates for Habitual Behavior. Neuron. 2016

Oldenburg IA, Sabatini BL. Antagonistic but Not Symmetric Regulation of Primary Motor Cortex by Basal Ganglia Direct and Indirect Pathways. Neuron. 2015; 86:1174–1181. [PubMed: 26050037]

Pennartz CM, Berke JD, Graybiel AM, Ito R, Lansink CS, van der Meer M, Redish AD, Smith KS, Voorn P. Corticostriatal Interactions during Learning, Memory Processing, and Decision Making. J Neurosci. 2009; 29:12831–12838. [PubMed: 19828796]

Planert H, Szydlowski SN, Hjorth JJ, Grillner S, Silberberg G. Dynamics of synaptic transmission between fast-spiking interneurons and striatal projection neurons of the direct and indirect pathways. J Neurosci. 2010; 30:3499–3507. [PubMed: 20203210]

Plenz D. When inhibition goes incognito: feedback interaction between spiny projection neurons in striatal function. Trends in neurosciences. 2003; 26:436–443. [PubMed: 12900175]

Qi J, Zhang S, Wang HL, Barker DJ, Miranda-Barrientos J, Morales M. VTA glutamatergic inputs to nucleus accumbens drive aversion by acting on GABAergic interneurons. Nat Neurosci. 2016

Reig R, Silberberg G. Multisensory integration in the mouse striatum. Neuron. 2014; 83:1200–1212. [PubMed: 25155959]

Reiner A, Shelby E, Wang H, Demarch Z, Deng Y, Guley NH, Hogg V, Roxburgh R, Tippett LJ, Waldvogel HJ, Faull RL. Striatal parvalbuminergic neurons are lost in Huntington's disease: implications for dystonia. Movement disorders: official journal of the Movement Disorder Society. 2013; 28:1691–1699. [PubMed: 24014043]

Rothwell PE, Hayton SJ, Sun GL, Fuccillo MV, Lim BK, Malenka RC. Input-and Output-Specific Regulation of Serial Order Performance by Corticostriatal Circuits. Neuron. 2015; 88:345–356. [PubMed: 26494279]

Schmitzer-Torbert NC, Redish AD. Task-dependent encoding of space and events by striatal neurons is dependent on neural subtype. Neuroscience. 2008; 153:349–360. [PubMed: 18406064]

Schultz W. Multiple reward signals in the brain. Nat Rev Neurosci. 2000; 1:199–207. [PubMed: 11257908]

Schultz W, Romo R. Role of primate basal ganglia and frontal cortex in the internal generation of movements. I. Preparatory activity in the anterior striatum. Exp Brain Res. 1992; 91:363–384. [PubMed: 1483512]

Shobe JL, Claar LD, Parhami S, Bakhurin KI, Masmanidis SC. Brain activity mapping at multiple scales with silicon microprobes containing 1,024 electrodes. Journal of Neurophysiology. 2015; 114:2043–2052. [PubMed: 26133801]

Silberberg G, Bolam JP. Local and afferent synaptic pathways in the striatal microcircuitry. Curr Opin Neurobiol. 2015; 33:182–187. [PubMed: 26051382]

Sippy T, Lapray D, Crochet S, Petersen CC. Cell-Type-Specific Sensorimotor Processing in Striatal Projection Neurons during Goal-Directed Behavior. Neuron. 2015; 88:298–305. [PubMed: 26439527]

Straub C, Saulnier JL, Begue A, Feng DD, Huang KW, Sabatini BL. Principles of Synaptic Organization of GABAergic Interneurons in the Striatum. Neuron. 2016; 92:84–92. [PubMed: 27710792]

Szydlowski SN, Pollak Dorocic I, Planert H, Carlen M, Meletis K, Silberberg G. Target selectivity of feedforward inhibition by striatal fast-spiking interneurons. J Neurosci. 2013; 33:1678–1683. [PubMed: 23345240]

Tang CC, Root DH, Duke DC, Zhu Y, Teixeria K, Ma S, Barker DJ, West MO. Decreased firing of striatal neurons related to licking during acquisition and overtraining of a licking task. J Neurosci. 2009; 29:13952–13961. [PubMed: 19890005]

Tecuapetla F, Jin X, Lima SQ, Costa RM. Complementary Contributions of Striatal Projection Pathways to Action Initiation and Execution. Cell. 2016; 166:703–715. [PubMed: 27453468]

Tepper JM, Tecuapetla F, Koos T, Ibanez-Sandoval O. Heterogeneity and diversity of striatal GABAergic interneurons. Frontiers in neuroanatomy. 2010; 4:150. [PubMed: 21228905]

Thorn CA, Atallah H, Howe M, Graybiel AM. Differential dynamics of activity changes in dorsolateral and dorsomedial striatal loops during learning. Neuron. 2010; 66:781–795. [PubMed: 20547134]

Thorn CA, Graybiel AM. Differential entrainment and learning-related dynamics of spike and local field potential activity in the sensorimotor and associative striatum. J Neurosci. 2014; 34:2845–2859. [PubMed: 24553926]

van den Pol AN, Yao Y, Fu LY, Foo K, Huang H, Coppari R, Lowell BB, Broberger C. Neuromedin B and gastrin-releasing peptide excite arcuate nucleus neuropeptide Y neurons in a novel transgenic mouse expressing strong Renilla green fluorescent protein in NPY neurons. J Neurosci. 2009; 29:4622–4639. [PubMed: 19357287]

van der Meer MA, Johnson A, Schmitzer-Torbert NC, Redish AD. Triple dissociation of information processing in dorsal striatum, ventral striatum, and hippocampus on a learned spatial decision task. Neuron. 2010; 67:25–32. [PubMed: 20624589]

Vicente AM, Galvao-Ferreira P, Tecuapetla F, Costa RM. Direct and indirect dorsolateral striatum pathways reinforce different action strategies. Current biology: CB. 2016; 26:R267–269. [PubMed: 27046807]

Xiong Q, Znamenskiy P, Zador AM. Selective corticostriatal plasticity during acquisition of an auditory discrimination task. Nature. 2015

Xu M, Li L, Pittenger C. Ablation of fast-spiking interneurons in the dorsal striatum, recapitulating abnormalities seen post-mortem in Tourette syndrome, produces anxiety and elevated grooming. Neuroscience. 2016; 324:321–329. [PubMed: 26968763]

Yamada H, Inokawa H, Hori Y, Pan X, Matsuzaki R, Nakamura K, Samejima K, Shidara M, Kimura M, Sakagami M, Minamimoto T. Characteristics of fast-spiking neurons in the striatum of behaving monkeys. Neuroscience research. 2016; 105:2–18. [PubMed: 26477717]

Yin HH, Knowlton BJ. The role of the basal ganglia in habit formation. Nat Rev Neurosci. 2006; 7:464–476. [PubMed: 16715055]

Yin HH, Mulcare SP, Hilario MR, Clouse E, Holloway T, Davis MI, Hansson AC, Lovinger DM, Costa RM. Dynamic reorganization of striatal circuits during the acquisition and consolidation of a skill. Nat Neurosci. 2009; 12:333–341. [PubMed: 19198605]

Yttri EA, Dudman JT. Opponent and bidirectional control of movement velocity in the basal ganglia. Nature. 2016

HIGHLIGHTS

- Examined PV cell function with large-scale neural recordings and optogenetics.
- Suppressing or over-activating striatal PV cells reduces projection neuron firing.
- A disynaptic inhibitory circuit couples PV cells to projection neurons.
- The influence of PV cells on striatal output and behavior declines with experience.

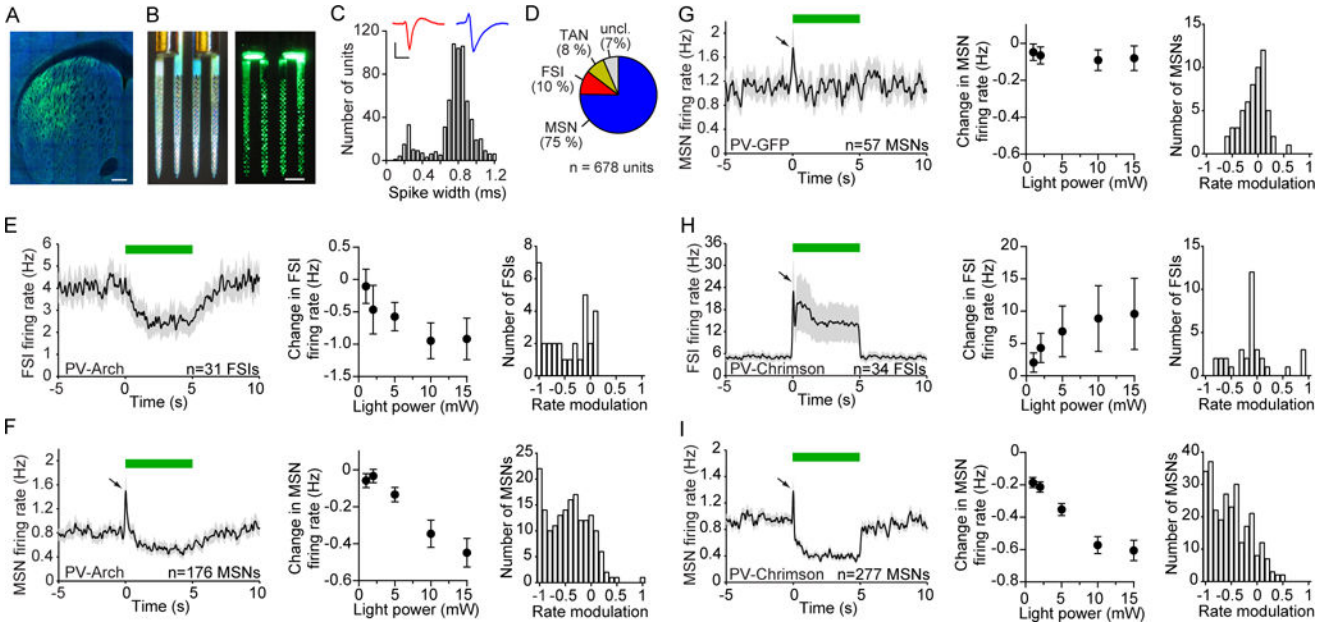

Figure 1. Striatal PV Interneurons Unidirectionally Control Spontaneous MSN activity

(A) Selective expression of Arch-GFP in PV cells in the dorsolateral striatum of PV-Cre mice. GFP (green) and NeuN (blue). Scale bar, 200 μm.

(B) Opto-microprobe device containing a 256 electrode silicon probe combined with 2 optical fibers. Left: view under ambient light. Right: view under laser illumination from the fibers. Scale bar, 200 μm.

(C) Distribution of trough-to-peak spike waveform duration of 678 striatal units recorded across 15 animals used in Figure 1. Narrow spiking units (less than 0.475 ms trough-to-peak duration) were mainly classified as putative FSIs, and wide spikes (greater than 0.55 ms trough-to-peak duration) were mainly classified as putative MSNs. Inset shows mean spike waveform of a representative FSI (red) and MSN (blue). Scale bars, 0.5 ms horizontal, 50 μV vertical.

(D) Percentage of putatively identified or unclassified striatal units.

(E) Response of 31 FSIs recorded *in vivo* to optical stimulation in Arch-expressing PV-Cre mice (PV-Arch). Left: The mean spontaneous firing rate was transiently reduced during 5 s continuous light delivery (green bar). Middle: The change in firing rate varied with optical fiber output power (one-way ANOVA, $F_{4,120} = 4.3$, $p = 0.003$). Right: Rate modulation index (RMI) distribution at 10 mW power. The median RMI was significantly different from zero (signed-rank test, $p < 0.0001$).

(F) Response of 176 MSNs to optical stimulation in PV-Arch mice. Left: After a brief excitatory response (black arrow) which was subsequently found to be an artifact, the mean activity decreased. Middle: The change in firing rate varied with optical fiber output power (one-way ANOVA, $F_{4,700} = 14$, $p < 0.0001$). Right: RMI distribution at 10 mW. The median RMI was significantly different from zero (signed-rank test, $p < 0.0001$).

(G) Response of 57 MSNs to optical stimulation in PV-GFP mice, which were not injected with optogenetic constructs. Left: There was no sustained change in firing relative to baseline. Middle: The change in firing rate did not significantly depend on optical fiber

output power (one-way ANOVA, $F_{4,224} = 0.1$, $p = 0.99$). Right: RMI distribution at 10 mW. The median RMI was not significantly different from zero (signed-rank test, $p = 0.77$).
(H) Response of 34 FSIs to optical stimulation in PV-Chrimson mice. Left: There was an increase in mean firing relative to baseline. Middle: The change in firing rate varied with optical fiber output power (one-way ANOVA, $F_{4,132} = 2.6$, $p = 0.04$). Right: RMI distribution at 10 mW. The median RMI was not significantly different from zero (signed-rank test, $p = 0.77$).
(I) Response of 277 MSNs to optical stimulation in PV-Chrimson mice. Left: There was a decrease in mean firing relative to baseline. Middle: The change in firing rate varied with optical fiber output power (one-way ANOVA, $F_{4,1104} = 33$, $p < 0.0001$). Right: RMI distribution at 10 mW. The median RMI was significantly different from zero (signed-rank test, $p < 0.0001$). See also Figures S1, S2. Data represent mean ± SEM.

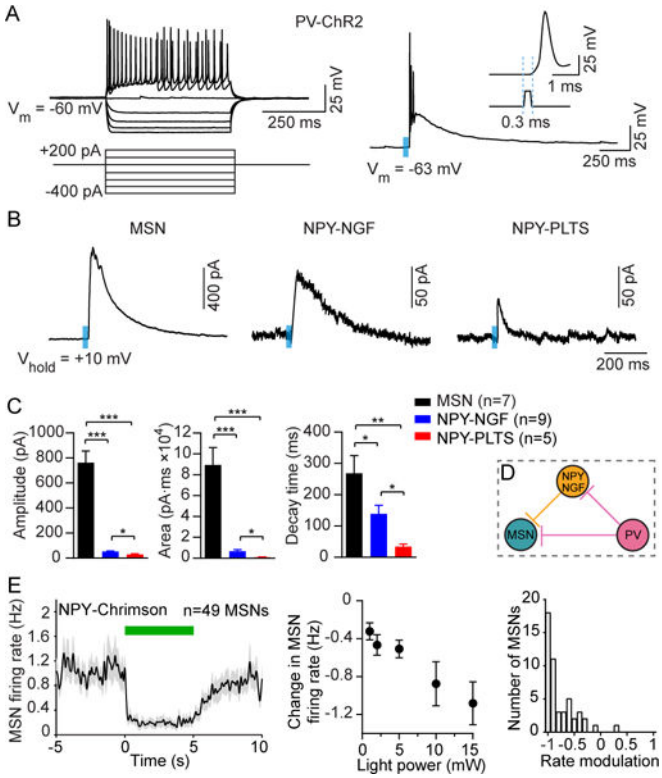

Figure 2. Characterization of a Disynaptic (PV-NPY-MSN) Inhibitory Microcircuit

(A) Striatal PV interneurons are fast-spiking interneurons (FSIs) that are characterized by a high firing frequency in response to depolarizing current injection (left). PV interneurons expressing ChR2 produced action potentials in response to blue light (right, 0.5 ms duration, 470 nm, 3 mW) with a latency of 0.3 ms (right, inset).

(B) Sample traces (average of 3 sweeps) of IPSC responses in MSNs, NPY-NGF, and NPY-PLTS cells after optical activation of PV interneurons.

(C) Mean evoked IPSC properties in MSNs and NPY interneurons after optical activation of PV interneurons. While the largest IPSC response magnitude was found to be in MSNs (n = 7), NPY-NGF cells (n = 9) produced IPSC responses with higher amplitudes (unpaired t-test, p = 0.02), larger areas (p = 0.015) and longer decay times (p = 0.018) compared to light-responsive NPY-PLTS cells (n = 5).

(D) Schematic model of microcircuitry of striatal PV interneurons coupled to MSNs both monosynaptically and disynaptically via NPY-NGF interneurons.

(E) Response of 49 MSNs recorded *in vivo* to optical stimulation in NPY-Chrimson mice. Left: The mean activity decreased during 5 s continuous light delivery (green bar). Middle: The change in firing rate varied with optical fiber output power (one-way ANOVA, $F_{4,192}$ = 7.7, p < 0.0001). Right: RMI distribution at 10 mW. The median RMI was significantly different from zero (signed-rank test, p < 0.0001). Data in *(C)* and *(E)* represent mean ± SEM.*p < 0.05;**p < 0.01; ****p < 0.0001.

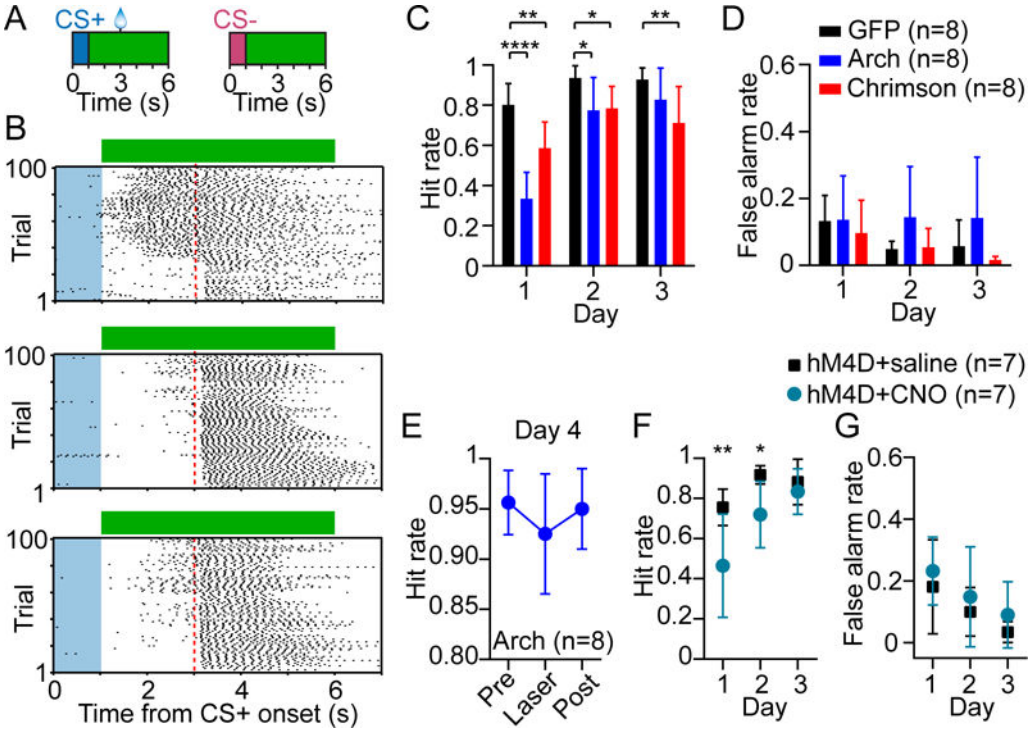

Figure 3. Striatal PV Interneurons Control Behavior during Early Reward Conditioning

(A) Stimulus-reward conditioning and optogenetic stimulation paradigm. Green bars denote the duration of bilateral optical stimulation.

(B) CS+ trial lick raster from day 1 of training of a PV-GFP (top), PV-Arch (middle), and PV-Chrimson (bottom) mouse receiving optical stimulation. Blue shaded area represents cue duration, green bar represents laser duration, dashed red line represents reward delivery time.

(C) Optogenetically suppressing or over-activating PV interneurons (n = 8 mice per group) selectively disrupted reward-anticipatory behavior (hit rate, two-way ANOVA, group effect: $F_{2,21} = 15$, $p < 0.0001$; time effect: $F_{2,42} = 43.7$, $p < 0.0001$). *Post hoc* Bonferroni's test revealed that hit rate was selectively reduced by PV suppression on day 1 and 2 of training relative to GFP controls, but was reduced across all days by PV over-activation.

(D) False alarm rate was not significantly affected by optogenetic manipulation (two-way ANOVA, group effect: $F_{2,21} = 1.7$, $p = 0.22$; time effect: $F_{2,42} = 6.6$, $p = 0.003$).

(E) In this cohort, PV-Arch animals (n = 8) were trained without laser for 3 days and tested with laser in the middle of day 4. The hit rate was not significantly affected (one-way ANOVA, $F_{2,14} = 2.5$, $p = 0.12$). Absolute maximum difference of the 95% confidence intervals = 0.07.

(F) Chemogenetically inhibiting PV interneurons using hM4D and CNO (n = 7 mice per group) selectively disrupted hit rate in the early stage of training (two-way ANOVA, group effect: $F_{1,12} = 8.2$, $p = 0.014$; time effect: $F_{2,24} = 20.8$, $p < 0.0001$). *Post hoc* Bonferroni's test revealed that hit rate was selectively reduced on day 1 and 2.

(G) False alarm rate was not significantly affected by chemogenetic inhibition (two-way ANOVA, group effect: $F_{1,12} = 1.4$, $p = 0.25$; time effect: $F_{2,24} = 7$, $p = 0.004$). Data in *(C–G)* are represented as mean ± SD. See also Figure S3. *p < 0.05; **p < 0.01; ****p < 0.0001.

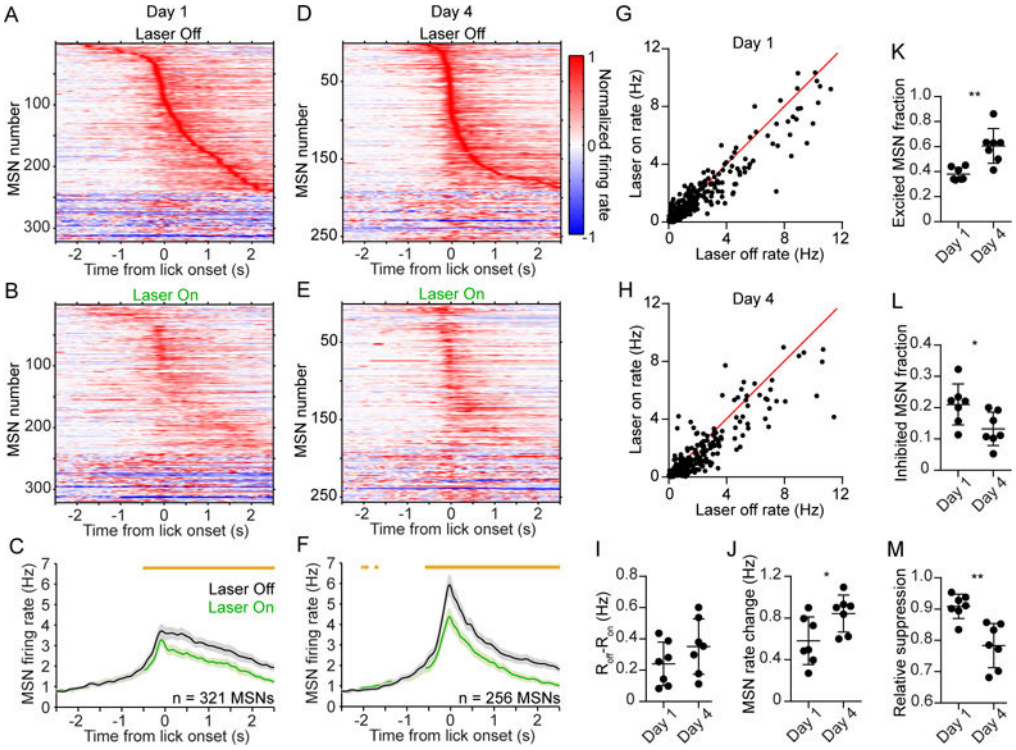

Figure 4. Experience Diminishes the Relative Influence of PV Interneurons on Preparatory MSN Activity

(A) Mean baseline-subtracted and normalized firing rate as a function of time of 321 MSNs recorded on day 1 of training, aligned to the first lick during hit trials without laser. Units are ordered by their latency to peak firing.

(B) Same as *(A)* but showing hit trials with laser. Note that the rate is normalized to the maximum firing during trials without laser. The order of units is the same as that of (A).

(C) Comparison of the mean firing rate of the population in *(A–B)* during laser off (black) and laser on (green) conditions. Orange bars above the plots denote time bins with significantly different off-on firing rate (paired t-test, $p < 0.01$).

(D) Mean baseline-subtracted and normalized firing rate as a function of time of 256 MSNs recorded on day 4 of training, aligned to the first lick during hit trials without laser. Units are ordered by their latency to peak firing.

(E) Same as *(D)* but showing trials with laser. Note that the rate is normalized to the maximum firing during trials without laser. The order of units is the same as that of *(D)*.

(F) Comparison of the mean firing rate of the population in *(D–E)* during laser off and laser on conditions. Data in *(C and F)* represent mean ± SEM.

(G) Comparison of median firing rate during a 1 s licking-preparatory period, between laser off and laser on conditions. The firing rate of the MSN population was significantly attenuated by optogenetic suppression of PV interneurons (Wilcoxon matched pairs signed-rank test, $p < 0.0001$). Each data point represents one MSN recorded on day 1 of training.

(H) Same as *(G)* but for day 4 of training. The firing rate of the MSN population was significantly attenuated by optogenetic suppression of PV interneurons (Wilcoxon matched pairs signed-rank test, $p < 0.0001$).

(I) The median level of MSN firing rate suppression per animal (R_{off}–R_{on}) did not significantly change from day 1 to day 4 (Mann-Whitney test, p = 0.26).
(J) The median level of preparatory MSN activity per animal increased from day 1 to day 4 (Mann-Whitney test, p = 0.026). The firing rate change is with respect to baseline activity.
(K) The fraction of MSNs per animal that were significantly excited during the preparatory period increased from day 1 to day 4 (Mann-Whitney test, p = 0.002).
(L) The fraction of MSNs per animal that were significantly inhibited during the preparatory period decreased from day 1 to day 4 (Mann-Whitney test, p = 0.019).
(M) The relative suppression factor per animal, which quantifies the change in MSN activity due to PV interneuron suppression relative to the total MSN preparatory activity, decreased from day 1 to day 4 (Mann-Whitney test, p = 0.002). Data in *(J–L)* are derived from non-laser trials, and each data point represents one animal (n = 7 mice per group). See also Figures S4, S5. *p < 0.05; **p < 0.01.

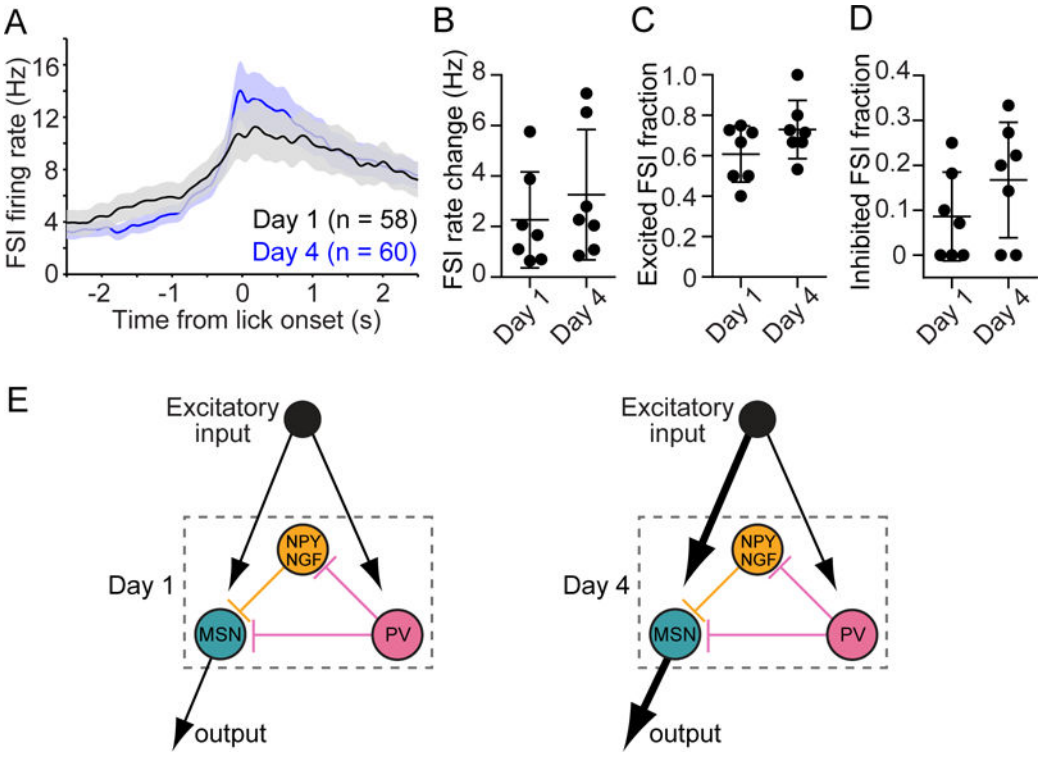

Figure 5. Experience does not Alter Preparatory FSI Activity

(A) Comparison of the mean firing rate as a function of time of the FSI population on day 1 and day 4 of training. Data are aligned to the first lick during hit trials without laser.

(B) The median level of preparatory FSI activity per animal did not significantly change from day 1 to day 4 (Mann-Whitney test, p = 0.38). The firing rate change is with respect to baseline activity.

(C) The fraction of FSIs per animal that were significantly excited during the preparatory period did not significantly change from day 1 to day 4 (Mann-Whitney test, p = 0.25).

(D) The fraction of FSIs per animal that were significantly inhibited during the preparatory period did not significantly change from day 1 to day 4 (Mann-Whitney test, p = 0.25). Data in *(A–D)* are derived from non-laser trials, and each data point in *(B–D)* represents one animal (n = 7 mice per group).

(E) Illustrative model of how the contribution of PV interneurons on MSN activity diminishes relative to other influences (here depicted as external excitatory input) in an experience-dependent manner. Left and right panels represent day 1 and day 4, respectively. Arrow thickness represents the relative strength of the designated pathway.